Supplementary Materials

Kinetic Parameter Estimation

Parametric forms of the standard one-tissue compartment (S1TC) model and adiabatic approximation to the tissue homogeneity (AATH) model time-activity curves can be derived by substituting Equations (2) and (3) into (4), respectively:

$$Q^{S1TC}(t) = v_b C_a(t - t_d) + (1 - v_b)K_1 \int_0^t C_a(\tau - t_d)e^{-k_2(t-\tau)}\, d\tau \quad (5)$$

$$Q^{AATH}(t) = F\left[\int_0^t C_a(\tau - t_d)\, d\tau - \int_0^{t-T_c} C_a(\tau - t_d)\, d\tau\right] + K_1 \int_0^{t-T_c} C_a(\tau - t_d)e^{-k_2(t-\tau-T_c)}\, d\tau \quad (6)$$

We interpreted the v_b term and F term as the intravascular distributions of the S1TC and AATH fitted time-activity curves, respectively, and the K_1 term as the extravascular distribution.

We used a basis function method[1,2] for all kinetic parameter estimation on time-activity curves of the dynamic scan's first two minutes. For the AATH model, basis functions were computed by using grid searched values of t_d from 0 to 50 s, T_c from 3 to 50 s, and 100 logarithmically spaced values of k_2 between 6×10^{-4} to 15 min^{-1}. The remaining linear parameters (F, K_1) were then estimated by a non-negative linear least squares algorithm.[3] A similar procedure was followed for the S1TC model but without T_c in the grid search and linearly estimating v_b and $(1 - v_b)\, K_1$. For both radiotracers, we assumed that whole-blood tracer activity was equal to that in blood plasma over the first two minutes of the dynamic PET scan. ^{11}C-butanol rapidly equilibrates uniformly between blood plasma and erythrocytes[4] and for ^{18}F-FDG, blood plasma is commonly approximated by the whole-blood image-derived arterial input function.

Tissue Segmentation

The lungs, renal cortex, spleen, and skeletal muscle (splenius capitis, psoas, thigh, calves), and bone marrow in the pelvis and lumbar vertebrae were manually delineated on 3D Slicer (Version 5.2)[5] by referencing a combination of the total-body CT, dynamic PET, and 0-2 minute static PET images. For the brain, we used a deep learning-based ^{18}F-FDG-PET/CT segmentation tool[6] to delineate the 83 brain regions of the Hammersmith atlas,[7] which were grouped to form masks of the cortical and subcortical grey matter, white matter, brainstem, and whole cerebellum. The grey and white matter in the cerebrum were distinguished by an Otsu threshold.[8] In participants with both ^{18}F-FDG and ^{11}C-butanol PET, FDG brain masks were

resampled to the ^{11}C-butanol-PET brain space by co-registering[9] the 0-2 minute static ^{18}F-FDG-PET brain image to that of the ^{11}C-butanol PET. Segmentations were visually inspected and manually adjusted as needed to avoid large vessels and organ boundaries where motion and spillover were more prevalent.

Supplementary Table 1. Range of average blood flow values reported in literature

Tissue	Range of Average Blood Flow Values [ml/min/cm^3]
Grey Matter	0.50–0.83[10–15]
White Matter	0.16–0.32[10–13]
Cerebellum	0.41–0.56[13,16,17]
Brainstem	0.31±0.10[18]
Bone Marrow	0.10–0.18[12,19]
Skeletal Muscle	0.03–0.05[12,20]
Spleen	1.3–1.7[12,21,22]
Renal Cortex	1.6–2.0[12,23]
Lungs	1.2–1.7[12,24–26]

Supplementary Table 2. Practical identifiability analysis of the adiabatic approximation to the tissue homogeneity (AATH) model

Tissue / Parameter	Noise Scale[27]	Mean (Standard Deviation) Error [%]				
		Blood Flow	K_1	E	v_b	T_c
Cortical GM	2.4	-0.6 (3.3)	0.1 (0.8)	0.9 (3.5)	0.0 (1.4)	0.9 (4.5)
Subcortical GM	11.8	-3.7 (12.6)	-0.5 (2.9)	6.1 (14.7)	2.9 (7.7)	12.0 (25.2)
White Matter	4.1	0.7 (6.1)	0 (1.9)	-0.2 (5.5)	0.0 (4.0)	0.1 (8.8)
Cerebellum	3.3	-0.3 (5.3)	0.0 (1.3)	0.6 (5.1)	0.2 (2.6)	1.0 (7.3)
Brainstem	10.0	0.6 (14.2)	-0.3 (3.4)	1.3 (13.3)	1.3 (8.5)	4.2 (21.8)
Bone Marrow	3.2	2.5 (4.2)	-1.3 (5.5)	-3.5 (4.6)	3.0 (21.8)	3.1 (23.6)
Skeletal Muscle	4.7	6.4 (8.7)	0.8 (6.7)	-4.4 (7.3)	4.8 (50.9)	3.6 (53.2)
Spleen	14.6	-0.8 (8.3)	-2.6 (9.1)	-1.4 (8.6)	11.6 (23.2)	15.8 (33.0)
Renal Cortex	15.3	0.4 (4.3)	0.2 (5.5)	-0.1 (5.9)	-0.1 (3.4)	-0.2 (6.2)
Lungs	7.1	0.0 (2.7)	1.3 (11.0)	1.4 (11.3)	0.0 (1.4)	0.1 (2.5)

A negative error indicates that the predicted value underestimated the true value. K_1 indicates the blood-to-tissue transport rate; E, extraction fraction; v_b, blood volume; T_c, mean vascular transit time; GM, grey matter

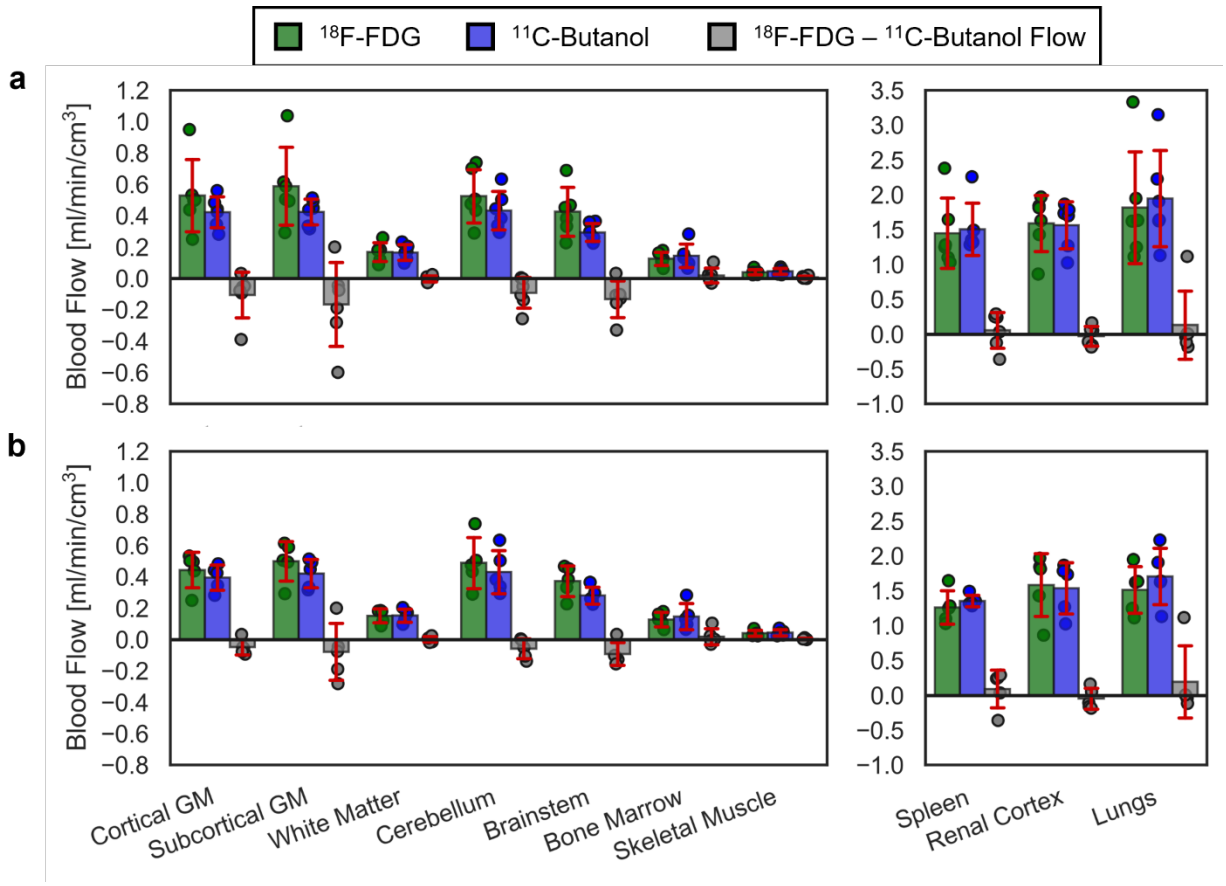

Supplementary Figure 1. Regional blood flow comparisons between our proposed ^{18}F-FDG method and the ^{11}C-butanol reference in six participants scanned with both radiotracers. (a) Including all six participants and (b) excluding the participant shown in Supplementary Figure 3.

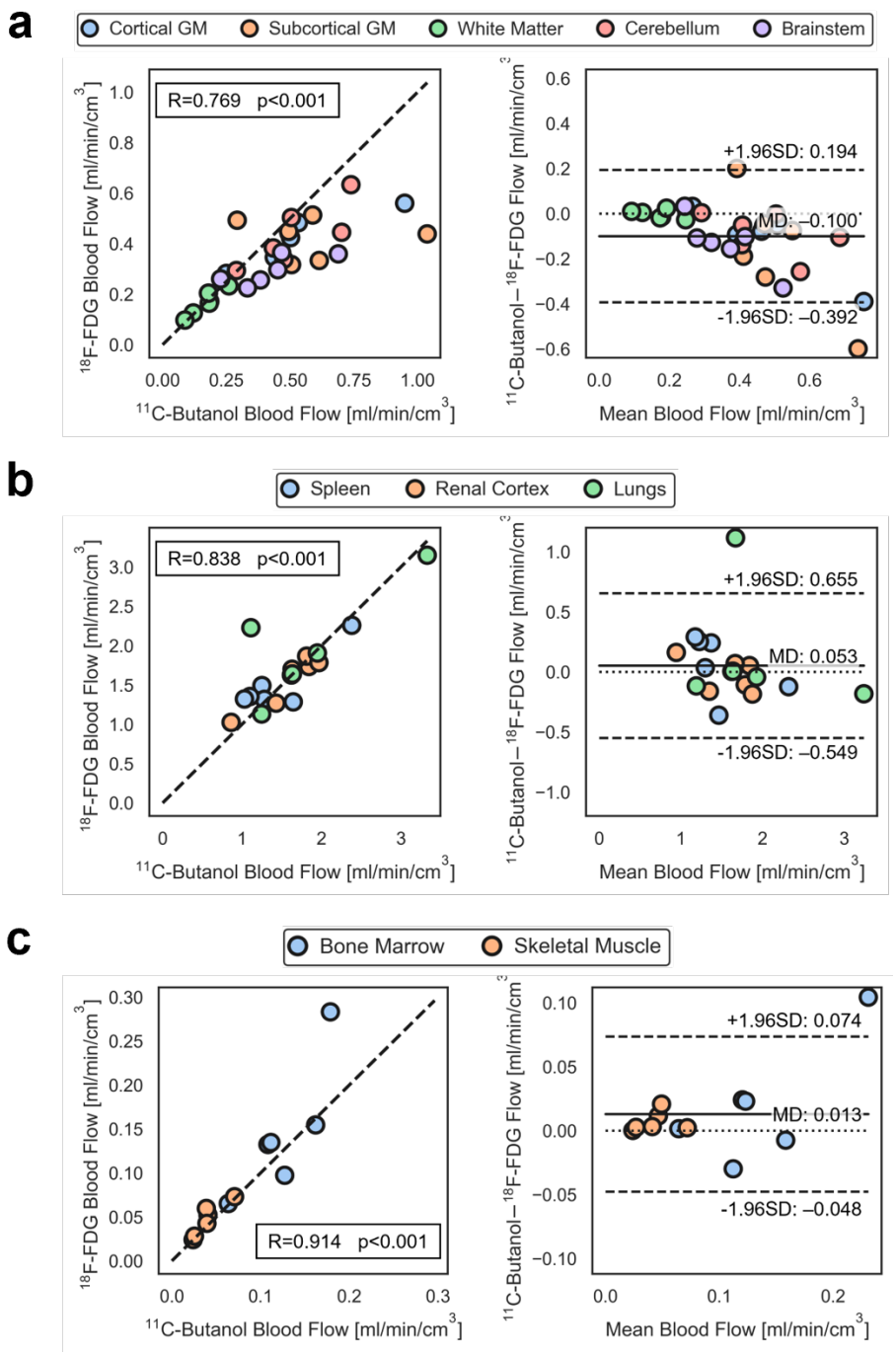

Supplementary Figure 2. Correlation (left) and Bland-Altman (right) plots comparing ^{18}F-fluorodeoxyglucose (FDG) blood flow with our proposed method against ^{11}C-butanol reference in the same subjects and stratified by (a) brain regions, (b) high blood flow tissues, and (c) low blood flow tissue. MD indicates mean difference; SD, standard deviation.

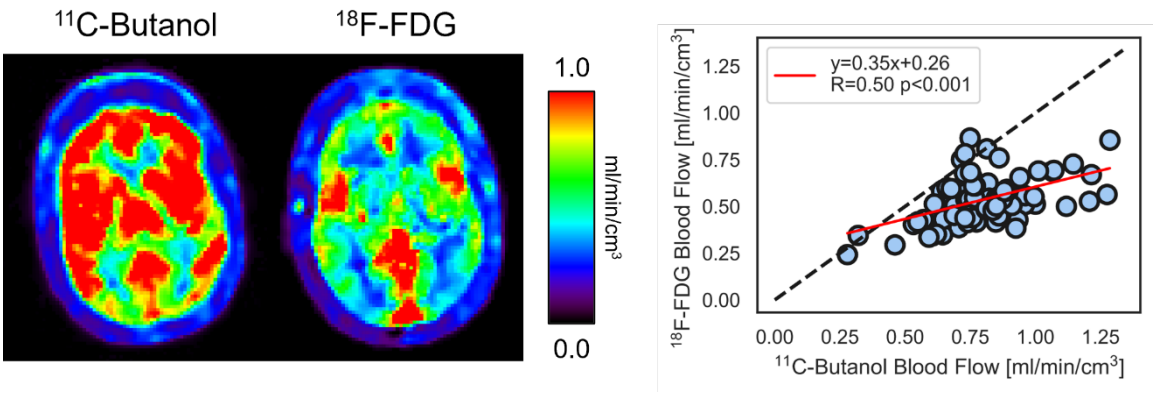

Supplementary Figure 3. ^{11}C-butanol and ^{18}F-FDG cerebral blood flow parametric images showed substantial differences in one participant scanned with both radiotracers. The correlation plot compares blood flow estimated with ^{11}C-butanol and ^{18}F-FDG across the 83 Hammersmith brain atlas regions.[7]

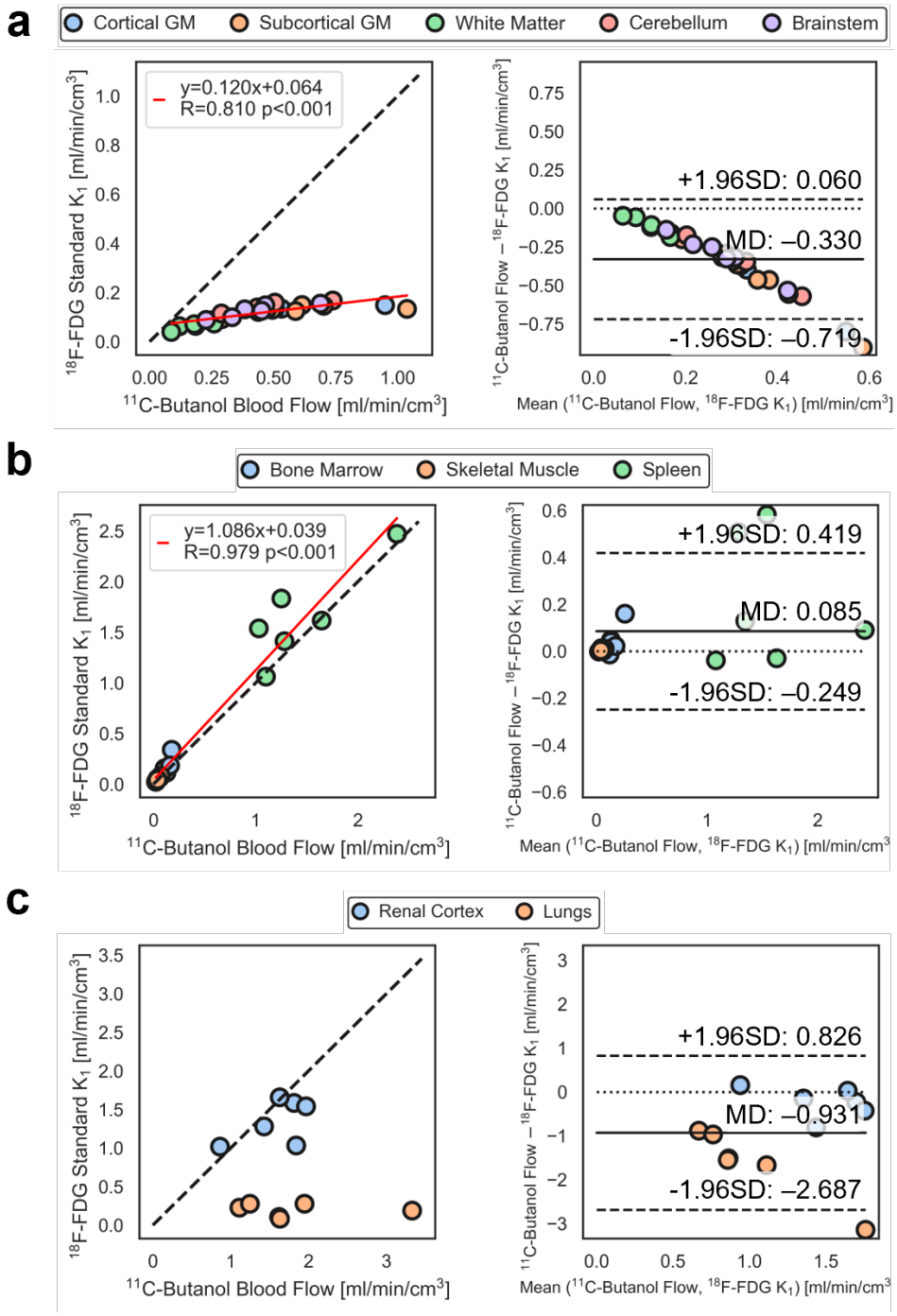

Supplementary Figure 4. Correlation (left) and Bland-Altman (right) plots comparing ^{11}C-butanol blood flow and ^{18}F-fluorodeoxyglucose (FDG) standard one-tissue compartment (S1TC) model K_1. Plots are stratified by (a) brain, (b) high extraction fraction, and (c) low to moderate extraction fraction (Table 1).

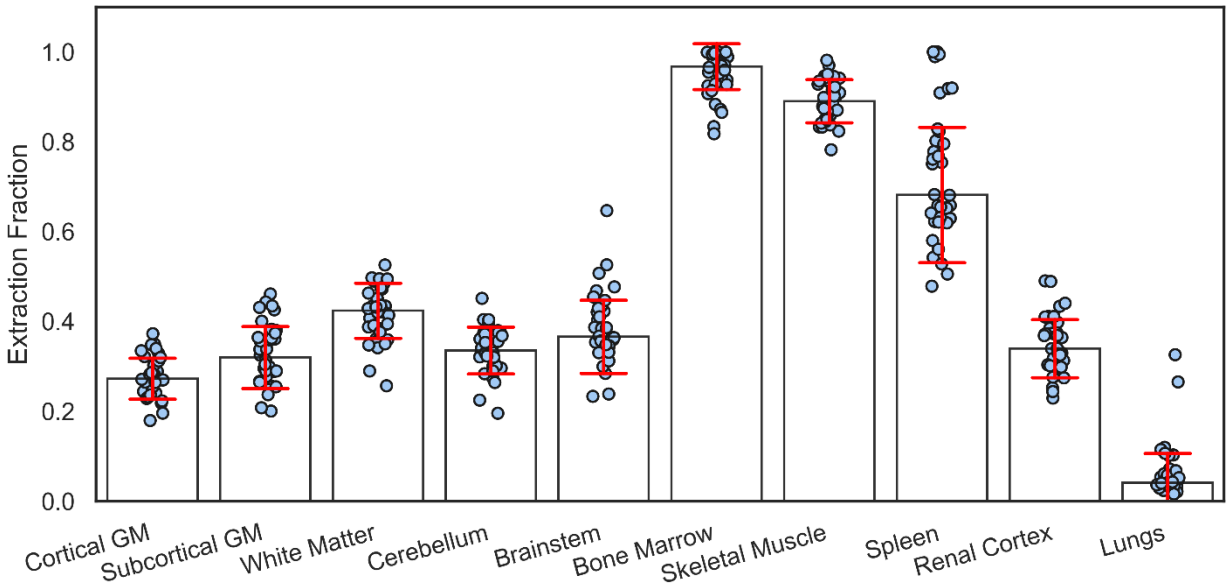

Supplementary Figure 5. Regional ^{18}F-fluorodeoxyglucose (FDG) extraction fractions estimated with the proposed method.

Supplementary References

1. Chung KJ, Abdelhafez YG, Spencer BA, et al. Quantitative PET imaging and modeling of molecular blood-brain barrier permeability. Published online July 27, 2024. doi:10.1101/2024.07.26.24311027

2. Gunn RN, Lammertsma AA, Hume SP, Cunningham VJ. Parametric Imaging of Ligand-Receptor Binding in PET Using a Simplified Reference Region Model. *NeuroImage*. 1997;6(4):279-287. doi:10.1006/nimg.1997.0303

3. Lawson CL, Hanson RJ. *Solving Least Squares Problems*. SIAM; 1995.

4. Knapp WolframH, Helus F, Oberdorfer F, et al. 11C-Butanol for imaging of the blood-flow distribution in tumor-bearing animals. *Eur J Nucl Med*. 1985;10-10(11-12). doi:10.1007/BF00252749

5. Fedorov A, Beichel R, Kalpathy-Cramer J, et al. 3D Slicer as an image computing platform for the Quantitative Imaging Network. *Magnetic Resonance Imaging*. 2012;30(9):1323-1341. doi:10.1016/j.mri.2012.05.001

6. Sundar LKS, Yu J, Muzik O, et al. Fully Automated, Semantic Segmentation of Whole-Body ^{18}F-FDG PET/CT Images Based on Data-Centric Artificial Intelligence. *J Nucl Med*. 2022;63(12):1941-1948. doi:10.2967/jnumed.122.264063

7. Hammers A, Allom R, Koepp MJ, et al. Three-dimensional maximum probability atlas of the human brain, with particular reference to the temporal lobe. *Human Brain Mapping*. 2003;19(4):224-247. doi:10.1002/hbm.10123

8. Otsu N. A Threshold Selection Method from Gray-Level Histograms. *IEEE Trans Syst, Man, Cybern*. 1979;9(1):62-66. doi:10.1109/TSMC.1979.4310076

9. Modat M, Cash DM, Daga P, Winston GP, Duncan JS, Ourselin S. Global image registration using a symmetric block-matching approach. *J Med Imag*. 2014;1(2):024003. doi:10.1117/1.JMI.1.2.024003

10. Quarles RP, Mintun MA, Larson KB, Markham J, MacLeod AM, Raichle ME. Measurement of Regional Cerebral Blood Flow with Positron Emission Tomography: A Comparison of [^{15}O]Water to [^{11}C]Butanol with Distributed-Parameter and Compartmental Models. *J Cereb Blood Flow Metab*. 1993;13(5):733-747. doi:10.1038/jcbfm.1993.94

11. Herscovitch P, Raichle ME, Kilbourn MR, Welch MJ. Positron Emission Tomographic Measurement of Cerebral Blood Flow and Permeability—Surface Area Product of Water Using [^{15}O]Water and [^{11}C]Butanol. *J Cereb Blood Flow Metab*. 1987;7(5):527-542. doi:10.1038/jcbfm.1987.102

12. Li EJ, López JE, Spencer BA, et al. Total-Body Perfusion Imaging with [^{11}C]-Butanol. *J Nucl Med*. Published online August 31, 2023:jnumed.123.265659. doi:10.2967/jnumed.123.265659

13. Leenders KL, Perani D, Lammertsma AA, et al. CEREBRAL BLOOD FLOW, BLOOD VOLUME AND OXYGEN UTILIZATION: NORMAL VALUES AND EFFECT OF AGE. *Brain*. 1990;113(1):27-47. doi:10.1093/brain/113.1.27

14. Berridge MS, Adler LP, Nelson AD, et al. Measurement of Human Cerebral Blood Flow with [^{15}O]Butanol and Positron Emission Tomography. *J Cereb Blood Flow Metab*. 1991;11(5):707-715. doi:10.1038/jcbfm.1991.127

15. Herzog H, Seitz RJ, Teilmann L, et al. Quantitation of Regional Cerebral Blood Flow with ^{15}O-Butanol and Positron Emission Tomography in Humans. *J Cereb Blood Flow Metab*. 1996;16(4):645-649. doi:10.1097/00004647-199607000-00015

16. Wayne Martin WR, Raichle ME. Cerebellar blood flow and metabolism in cerebral hemisphere infarction. *Ann Neurol*. 1983;14(2):168-176. doi:10.1002/ana.410140203

17. Gaillard WD, Zeffiro T, Fazilat S, DeCarli C, Theodore WH. Effect of Valproate on Cerebral Metabolism and Blood Flow: An 18F-2-Deoxyglusose and 15O Water Positron Emission Tomography Study. *Epilepsia*. 1996;37(6):515-521. doi:10.1111/j.1528-1157.1996.tb00602.x

18. Warnert EA, Harris AD, Murphy K, et al. *In vivo* Assessment of Human Brainstem Cerebrovascular Function: A Multi-Inversion Time Pulsed Arterial Spin Labelling Study. *J Cereb Blood Flow Metab*. 2014;34(6):956-963. doi:10.1038/jcbfm.2014.39

19. Kahn D, Weiner G, Ben-Haim S, et al. Positron emission tomographic measurement of bone marrow blood flow to the pelvis and lumbar vertebrae in young normal adults [published erratum appears in Blood 1994 Nov 15;84(10):3602]. *Blood*. 1994;83(4):958-963. doi:10.1182/blood.V83.4.958.958

20. Bertoldo A, Peltoniemi P, Oikonen V, Knuuti J, Nuutila P, Cobelli C. Kinetic modeling of [^{18}F]FDG in skeletal muscle by PET: a four-compartment five-rate-constant model. *American Journal of Physiology-Endocrinology and Metabolism*. 2001;281(3):E524-E536. doi:10.1152/ajpendo.2001.281.3.E524

21. Taniguchi H, Yamaguchi A, Kunishima S, et al. Using the spleen for time-delay correction of the input function in measuring hepatic blood flow with oxygen-15 water by dynamic PET. *Ann Nucl Med*. 1999;13(4):215-221. doi:10.1007/BF03164895

22. Oguro A, Taniguchi H, Koyama H, et al. Quantification of human splenic blood flow (Quantitative measurement of splenic blood flow with H2 15O and a dynamic state method: 1). *Ann Nucl Med*. 1993;7(4):245-250. doi:10.1007/BF03164705

23. Kudomi N, Koivuviita N, Liukko KE, et al. Parametric renal blood flow imaging using [15O]H2O and PET. *Eur J Nucl Med Mol Imaging*. 2009;36(4):683-691. doi:10.1007/s00259-008-0994-8

24. Hopkins SR, Wielpütz MO, Kauczor HU. Imaging lung perfusion. *Journal of Applied Physiology*. 2012;113(2):328-339. doi:10.1152/japplphysiol.00320.2012

25. Matsunaga K, Yanagawa M, Otsuka T, et al. Quantitative pulmonary blood flow measurement using 15O-H2O PET with and without tissue fraction correction: a comparison study. *EJNMMI Res*. 2017;7(1):102. doi:10.1186/s13550-017-0350-8

26. Schuster DP, Kaplan JD, Gauvain K, Welch MJ, Markham J. Measurement of regional pulmonary blood flow with PET. *J Nucl Med*. 1995;36(3):371-377.

27. Zuo Y, Sarkar S, Corwin MT, Olson K, Badawi RD, Wang G. Structural and practical identifiability of dual-input kinetic modeling in dynamic PET of liver inflammation. *Phys Med Biol*. 2019;64(17):175023. doi:10.1088/1361-6560/ab1f29